

New H₂O masers in Seyfert and FIR bright galaxies [★]

C. Henkel¹, A. B. Peck², A. Tarchi^{3,4}, N. M. Nagar^{5,6,7}, J. A. Braatz⁸, P. Castangia^{4,9}, and L. Moscadelli⁴

¹ Max-Planck-Institut für Radioastronomie, Auf dem Hügel 69, D-53121 Bonn, Germany

² Harvard-Smithsonian Center for Astrophysics, SAO/SMA Project, 654 N. A'ohoku Pl., Hilo, HI 96720, USA

³ Istituto di Radioastronomia, CNR, Via Gobetti 101, I-40129-Bologna, Italy

⁴ INAF-Osservatorio Astronomico di Cagliari, Loc. Poggio dei Pini, Strada 54, I-09012 Capoterra (CA), Italy

⁵ INAF, Arcetri Observatory, Largo E. Fermi 5, I-50125 Florence, Italy

⁶ Kapteyn Instituut, Postbus 800, NL-9700 AV Groningen, The Netherlands

⁷ Astronomy Group, Departamento de Física, Universidad de Concepción, Casilla 160-C, Concepción, Chile

⁸ National Radio Astronomy Observatory, P.O. Box 2, Green Bank, WV 24944, USA

⁹ Università di Cagliari, Dipartimento di Fisica, Cittadella Universitaria, I-09012 Capoterra (CA), Italy

Received 14 October 2004 / Accepted 16 February 2005

Abstract. Using the Effelsberg 100-m telescope, detections of four extragalactic water vapor masers are reported. Isotropic luminosities are ~ 50 , 1000, 1, and $230 L_{\odot}$ for Mrk 1066 (UGC 2456), Mrk 34, NGC 3556, and Arp 299, respectively. Mrk 34 contains by far the most distant and one of the most luminous water vapor megamasers so far reported in a Seyfert galaxy. The interacting system Arp 299 appears to show two maser hotspots separated by approximately $20''$. With these new results and even more recent data from Braatz et al. (2004), the detection rate in our sample of Seyferts with known jet-Narrow Line Region interactions becomes 50% (7/14), while in star forming galaxies with high ($S_{100\mu\text{m}} > 50 \text{ Jy}$) far infrared fluxes the detection rate is 22% (10/45). The jet-NLR interaction sample may not only contain ‘jet-masers’ but also a significant number of accretion ‘disk-masers’ like those seen in NGC 4258. A statistical analysis of 53 extragalactic H₂O sources (excluding the Galaxy and the Magellanic Clouds) indicates (1) that the correlation between IRAS Point Source and H₂O luminosities, established for individual star forming regions in the galactic disk, also holds for AGN dominated megamaser galaxies, (2) that maser luminosities are not correlated with $60\mu\text{m}/100\mu\text{m}$ color temperatures and (3) that only a small fraction of the luminous megamasers ($L_{\text{H}_2\text{O}} > 100 L_{\odot}$) detectable with 100-m sized telescopes have so far been identified. The H₂O luminosity function (LF) suggests that the number of galaxies with $1 L_{\odot} < L_{\text{H}_2\text{O}} < 10 L_{\odot}$, the transition range between ‘kilomasers’ (mostly star formation) and ‘megamasers’ (active galactic nuclei), is small. The overall slope of the LF, ~ -1.5 , indicates that the number of detectable masers is almost independent of their luminosity. If the LF is not steepening at very high maser luminosities and if it is possible to find suitable candidate sources, H₂O megamasers at significant redshifts should be detectable even with present day state-of-the-art facilities.

Key words. Masers – Galaxies: active – Galaxies: Jets – Galaxies: Seyfert – Galaxies: starburst – Radio lines: galaxies

1. Introduction and sample selection

Extragalactic water vapor masers, observed through the 22 GHz ($\lambda \sim 1.3 \text{ cm}$) $J_{\text{KaKc}} = 6_{16} - 5_{23}$ line of ortho-H₂O that traces warm ($T_{\text{kin}} \gtrsim 400 \text{ K}$) and dense ($n(\text{H}_2) \gtrsim 10^7 \text{ cm}^{-3}$) molecular gas (e.g. Kylafis & Norman 1987, 1991; Fiebig & Güsten 1989), are primarily seen as a means to probe nuclear accretion disks in active galaxies.

The best known source, NGC 4258, shows a thin, slightly warped, nearly edge-on Keplerian disk of subparsec scale enclosing a central mass of $\sim 4 \times 10^7 M_{\odot}$ (e.g. Greenhill et al. 1995; Miyoshi et al. 1995; Herrnstein et al. 1999).

There is evidence, however, for additional classes of extragalactic H₂O masers. There are sources in which at least a part of the H₂O emission appears to be the result of an interaction between the nuclear radio jet and an encroaching molecular cloud (e.g. Mrk 348; Peck et al. 2003).

Most of the nuclear water vapor sources are characterised by (isotropic) $L_{\text{H}_2\text{O}} > 10 L_{\odot}$ and are classified as ‘megamasers’. H₂O masers associated with prominent star

Send offprint requests to: C. Henkel, e-mail: chenkel@mpifr-bonn.mpg.de

[★] Based on observations with the 100-m telescope of the MPIfR (Max-Planck-Institut für Radioastronomie) at Effelsberg.

forming regions similar to those seen in the Galaxy (e.g. in M 33; Greenhill et al. 1993) are less luminous and comprise the majority of known ‘kilomaser’ ($L_{\text{H}_2\text{O}} \lesssim 10 L_\odot$).

Providing bright, almost point-like hotspots, H₂O masers are ideal probes for Very Long Baseline Interferometry (VLBI). A broad variety of astrophysical studies is possible. This includes the determination of geometric distances and 3-dimensional velocity vectors of galaxies, masses of nuclear engines, maps of accretion disks and physics of nuclear jet-molecular cloud interaction (for recent reviews, see Greenhill 2002, 2004; Maloney 2002; Henkel & Braatz 2003; Morganti et al. 2004; Henkel et al. 2005).

So far, almost 1000 active galaxies have been surveyed. In order to detect a large number of strong maser sources that could help to elucidate the nuclear environment of their parent galaxies and their geometric distance, typical detection limits were several 10 mJy or more, resulting in detection rates between zero (e.g. Henkel et al. 1998) and a few percent (e.g. Henkel et al. 1984; Braatz et al. 1996, Greenhill et al. 2002). The low detection rates are probably the result of the limited sensitivity of the surveys, rather than an intrinsic lack of extragalactic H₂O masers. The technology exists to do deeper searches; what is required is a set of criteria to narrow the list of candidates from all nearby galaxies to a manageable few. Here we present the results of two quite different, but equally successful, deep searches (to estimate distances, $H_0 = 75 \text{ km s}^{-1} \text{ Mpc}^{-1}$ is used, whenever possible, throughout the paper).

Sample 1: The targets of the first sample (hereafter ‘jet-maser’ sample) have been selected from a collection of Seyfert galaxies with declination $> -30^\circ$ in which both the inclination of the host galaxy and the linear extent of the radio source are known (Nagar & Wilson 1999). To maximize the detection rate, we have chosen galaxies which either show evidence at optical wavelengths of interaction between the radio jet and clouds in the narrow line region, or have a face-on ($i < 35^\circ$) galaxy disk and extended pc to 100-pc scale radio structures, possibly suggesting that both the disk of the galaxy and the radio jet should be fairly close to the plane of the sky. This combination of geometries increases the probability that the radio jet lies close to the disk of the galaxy, thus increasing the likelihood of interaction between the radio jet and the galaxy interstellar medium (ISM). Indeed, two of the four ‘jet-maser’ sources known prior to this study, NGC 1068 (Gallimore et al. 2001) and Mrk 348 (Peck et al. 2003) appear in the parent sample and fit the above criteria. The complete list of 14 jet-maser target sources is given in Table 1.

Sample 2: The second sample (hereafter ‘far infrared maser’ or ‘FIR-maser’ sample) is comprised of all galaxies with declination $> -30^\circ$ and IRAS point source flux density $S_{100\mu\text{m}} > 50 \text{ Jy}$ (e.g. Fullmer & Lonsdale 1989). The

same criteria were already used by Henkel et al. (1986; hereafter HWB) to perform a first FIR-flux-based survey in which they detected a new maser in the galaxy IC 10. Recently we have detected masers in IC 342 (Tarchi et al. 2002a) and NGC 2146 (Tarchi et al. 2002b), which were previously undetected although they were included in the sample of HWB. We attribute this result to an occasional flare (IC 342) and to an improvement in the Effelsberg receiver and backend systems (NGC 2146). This motivated us to re-observe the list of previously undetected targets. The list of sources was compiled using the IRAS Point Source Catalog (e.g. Fullmer & Lonsdale 1989) and is shown in Table 2. There is a total of 45 sources, the great majority of them being spiral galaxies. Two of these already known to show maser emission, IC 342 and NGC 2146, were reobserved.

2. Observations

The target sources of the two samples were measured in the $6_{16} - 5_{23}$ line of H₂O (rest frequency: 22.23508 GHz) with the 100-m telescope of the MPIfR at Effelsberg on various occasions between June 2001 and April 2004. The full width to half power beamwidth was $\sim 40''$ and the pointing accuracy was in most cases better than $10''$ (see also Sect. 4.2.3). A dual channel HEMT receiver provided system temperatures of 130–180 K on a main beam brightness temperature scale. The observations were carried out in a dual beam switching mode with a beam throw of $2'$ and a switching frequency of $\sim 1 \text{ Hz}$. The autocorrelator backend was split into eight bands of width 40 or 80 MHz and 512 or 256 channels each that could individually be shifted in frequency by up to $\pm 250 \text{ MHz}$ relative to the recessional velocity of the galaxy. This yielded channel spacings of ~ 1 or $\sim 4 \text{ km s}^{-1}$. A few spectra were also taken with two bands of 20 MHz and 4096 channels each. The resulting channel spacing was then $\sim 0.07 \text{ km s}^{-1}$. Flux calibration was obtained by measurements of W3(OH) (for the flux, see Mauersberger et al. 1988). Gain variations as a function of elevation were taken into account (see Eq. 1 of Gallimore et al. 2001) and the 1σ flux calibration error is expected to not exceed $\pm 10\%$.

3. Results

From the jet-maser sample, we have detected two new megamasers, Mrk 1066 and Mrk 34. The FIR-maser sample also yields two new detections, a megamaser (Arp 299) and a kilomaser (NGC 3556). Line profiles are shown in Figs. 1–6. Line parameters including recessional velocity and (isotropic) H₂O luminosity are given in Table 3. Properties of the detected galaxies are discussed below.

3.1. Mrk 1066 (UGC 2456)

Mrk 1066 is a FIR luminous ($L_{\text{FIR}} \sim 7 \times 10^{10} L_\odot$) SB0+ galaxy, containing a double nucleus (e.g. Gimeno et al. 2004). It is one of the few early-type galaxies that have

Table 1. ‘Jet-maser’ observations

Source ^{a)}	Seyfert	R.A.	Dec.	$V_{\text{sys}}^{\text{b)}$	V -range	rms	Channel Width	Epoch ^{c)}
	(Type)	(J2000)	(J2000)	(cz)	(km s ⁻¹)	(mJy)	(km s ⁻¹)	
<i>Mrk 348</i> (NGC 262) ^{d)}	2	00 48 47.1	31 57 25	4500				
<i>Mrk 1157</i> (NGC 591) ^{d)}	2	01 33 31.2	35 39 56	4550	4050,5080	8	1.1	0302
<i>Mrk 573</i>	2	01 43 57.8	02 20 59	5175	4700,5700	13	1.1	0302
<i>NGC 1068</i> ^{d)}	1.8	02 42 40.7	-00 00 48	1135				
Mrk 1066 ^{d)}	2	02 59 58.6	36 49 14	3605	see Table 3			
MCG 8-11-11	1.5	05 54 53.6	46 26 21	6140	5650,6680	6	1.1	0302
<i>Mrk 3</i> ^{d)}	2	06 15 36.3	71 02 15	4050	3600,4480	5	4.2	0701
					3570,4580	9	1.1	0302
Mrk 79	1.2	07 42 32.8	49 48 35	6650	6160,7190	8	1.1	0302
Mrk 34 ^{d)}	2	10 34 08.6	60 01 52	15140	see Table 3			
NGC 3516	1.2	11 06 47.4	72 34 07	2650	2160,3180	9	1.1	0302
<i>NGC 4151</i> ^{d)}	1.5	12 10 32.6	39 24 21	1000	0,2000	3	4.3	0300
NGC 5135	2	13 25 43.8	-29 50 02	4110	3630,4650	18	1.1	0302
Mrk 270 (NGC 5283)	2	13 41 05.7	67 40 21	3120	2640,3650	9	1.1	0302
Mrk 1126 (NGC 7450)	1.5	23 00 47.8	-12 55 06	3190	2700,3730	9	1.1	0302

a) Source names in italics: previously detected sources; bold-faced: newly detected sources

b) V_{sys} : Systemic velocity

c) Epoch: given are the month (first two digits) and the year (last two digits)

d) Mrk 348: Falcke et al. (2000); Mrk 1157: Braatz et al. (2004); NGC 1068: Claussen et al. (1984); Mrk 1066: this paper, for a more recent independent detection see Braatz et al. (2004); Mrk 3: Braatz et al. (2004); Mrk 34: this paper; NGC 4151: Braatz et al. (2004)

been detected in CO (see Henkel & Wiklind 1997; note that their FIR luminosity (their Table II) is too low). Its systemic velocity is 3605 km s⁻¹ (see Table 1), corresponding to a distance of ~ 50 Mpc. The inclination angle is 42° (Whittle 1992). Hubble Space Telescope (HST) imaging of the nuclear region (Bower et al. 1995) shows a jet-like feature in a narrow-band image which includes [OIII] and H β . The distribution is bipolar, oriented at $\sim 315^\circ$, and extending to an angular radius of $\sim 1''.5$, with emission from the north-western side being dominant. In H α and [NII], the jet is equally prominent on both sides of the nucleus. The 3.6 cm radio continuum emission (Nagar et al. 1999) is extended along the same axis over $\sim 2''.5$.

There is a strong narrow maser spike at 3636 km s⁻¹ with a full width to half maximum linewidth of less than 2 km s⁻¹ (Figs. 1 and 2) and a peak flux density of 80 mJy. The spike becomes narrower between March 7 and 10, 2002, appears to be unresolved in frequency in May and reaches only ~ 50 mJy in September. It seems that a gradual decrease of the linewidth is finally accompanied by a decrease in peak flux density. At a distance of ~ 50 Mpc, isotropic luminosities reach $\sim 10 L_\odot$. A second much wider component, at ~ 3550 km s⁻¹, has a peak flux density of 10–20 mJy and an isotropic luminosity of $\sim 40 L_\odot$.

3.2. Mrk 34

Mrk 34 (IRAS 10309+6017), another luminous ($\sim 10^{11} L_\odot$) FIR source, is a distant Seyfert 2 galaxy ($z=0.0505$, $D \sim 200$ Mpc; Falcke et al. 1998). The optical galaxy is characterized as having an inclination angle of 57° in Whittle (1992), though a second generation Digital Sky Survey (DSS) image shows the galaxy to be compact, with poorly defined outer isophotes (Nagar & Wilson

1999). The radio emission has an extended structure ($\sim 2''.5$; Ulvestad & Wilson 1984), and strong evidence for an interaction between the radio jet and NLR clouds has been found by Falcke et al. (1998).

Mrk 34 is one of the most distant and most luminous H₂O megamasers ever detected. The maser shows two or three distinct spectral features (Figs. 3 and 4). One is centered at a velocity of ~ 14840 km s⁻¹, another at ~ 15770 km s⁻¹, and a third one is tentatively seen at ~ 14665 km s⁻¹. Peak flux densities are up to 10 mJy and total isotropic luminosities are $\sim 1000 L_\odot$.

3.3. NGC 3556 (M 108)

NGC 3556 is an edge-on spiral galaxy located at a distance of ~ 12 Mpc. Its FIR luminosity, $L_{\text{FIR}} \sim 10^{10} L_\odot$, is similar to that of the Milky Way. Radio continuum, HI and X-ray data indicate a violent disk halo interaction, including a prominent radio halo (e.g. de Bruyn & Hummel 1979), large HI extensions possibly delineating expanding supershells (King & Irwin 1997), compact radio continuum sources, likely representing supernova remnants (Irwin et al. 2000), and extraplanar diffuse X-ray emission (Wang et al. 2003). ¹²CO and HCN observations (Gao & Solomon 2004) indicate a substantial molecular gas content. No OH maser was detected (Unger et al. 1986).

With a peak flux density of 20–40 mJy, the H₂O maser has an isotropic luminosity of $\sim 1 L_\odot$. Only one velocity component is seen. The profiles are shown in Fig. 5.

3.4. Arp 299 (Mrk 171)

Arp 299 is a merging system at $D \sim 40$ Mpc, composed of two main sources, IC 694 and NGC 3690 (for an al-

Table 2. ‘FIR-maser’ observations

Source ^{a)}	R.A.	Dec.	V_{sys}	$S_{100\mu\text{m}}^{\text{b)}$	V -range	rms	Channel Width	Epoch ^{c)}
	(J2000)	(J2000)	(cz)	(Jy)	(km s ⁻¹)	(mJy)	(km s ⁻¹)	
<i>IC 10</i> ^{d)}	00 20 27.0	59 17 29	-350	71				
<i>NGC 253</i> ^{d)}	00 47 33.1	-25 17 18	240	1045				
NGC 660	01 43 01.6	13 38 35	850	104	620,1100	7	1.1	0601
					0,1780	10	4.2	0302
NGC 891	02 22 33.4	42 20 57	525	148	320,900	20	1.1	0601
NGC 972	02 34 12.9	29 18 48	1540	65	700,2470	9	4.3	0302
					860,2080	20	1.1	0302
NGC 1055	02 41 45.4	00 26 35	1000	60	800,1250	17	1.1	1203
					450,1600	17	1.1	0404
Maffei 2	02 41 55.1	59 36 11	-35	227	-250,210	12	1.1	0601
					-250,200	15	1.1	0302
<i>NGC 1068</i> ^{d)}	02 42 40.7	-00 00 48	1135	240				
NGC 1084	02 46 00.0	-07 34 37	1405	55	930,1940	20	1.1	0103
<i>IC 342</i> ^{d)}	03 46 48.6	68 05 46	40	128	-190,300	12	1.1	0601
					-150,300	9	1.1	0302
UGC 02855	03 48 22.6	70 07 57	1200	79	980,1460	9	1.1	0601
NGC 1569	04 30 46.8	64 51 02	100	52	-100,190	12	1.1	0601
<i>NGC 2146</i> ^{d)}	06 18 39.6	78 21 19	900	187	500,1190	7	1.1	0302
NGC 2403	07 37 37.6	71 19 32	130	56	-100,400	9	1.1	0601
NGC 2559	08 17 06.0	-27 27 27	1560	66	1080,2090	20	1.1	0103
NGC 2903	09 32 10.1	21 30 04	550	104	100,1100	7	4.2	0701
<i>NGC 3034</i> ^{d)}	09 55 52.2	69 40 47	200	1145				
<i>NGC 3079</i> ^{d)}	10 01 57.8	55 40 47	1120	89				
NGC 3521	11 05 48.6	-00 02 09	850	85	320,1340	29	1.1	0302
NGC 3556 ^{d)}	11 11 31.2	55 40 25	700	61	see Table 3			
NGC 3627	11 20 15.0	12 59 30	725	106	300,1250	8	4.2	0701
NGC 3628	11 20 17.0	13 35 20	842	103	400,1380	7	4.2	0701
Arp 299 ^{d)}	11 28 31.9	58 33 45	3120	111	see Table 3			
NGC 4038	12 01 52.8	-18 51 54	1640	76	1020,2300	28	1.1	0502
NGC 4088	12 05 34.2	50 32 21	750	52	280,1280	16	1.1	0302
NGC 4102	12 06 23.1	52 42 39	850	69	600,1100	17	1.1	0601
NGC 4254	12 18 49.5	14 25 00	2400	72	2000,2930	6	4.3	0701
NGC 4303	12 21 54.9	04 28 25	1565	62	1080,2100	13	1.1	0302
NGC 4321	12 22 54.9	15 49 20	1570	58	1100,2100	12	1.1	0302
NGC 4414	12 26 27.1	31 13 24	700	68	230,1250	17	1.1	0302
NGC 4490	12 30 36.1	41 38 34	560	78	60,1100	17	1.1	0302
NGC 4501	12 31 59.1	14 25 14	2278	55	1800,2800	10	1.1	0103
NGC 4527	12 34 08.5	02 39 10	1735	64	1240,2260	15	1.1	0302
NGC 4631	12 42 07.9	32 32 26	600	120	200,1100	7	4.2	0701
NGC 4666	12 45 08.7	-00 27 41	1500	77	1050,2050	10	1.1	0103
NGC 4736	12 50 53.0	41 07 13	300	105	-150,820	5	4.2	0701
NGC 4826	12 56 43.7	21 40 52	400	76	-80,940	11	1.1	0103
NGC 5005	13 10 56.3	37 03 33	950	59	450 1470	13	1.1	0302
NGC 5055	13 15 49.3	42 01 49	500	101	30,1030	12	1.1	0302
<i>NGC 5194</i> ^{d)}	13 29 52.7	47 11 42	450	123				
NGC 5236	13 37 00.7	-29 51 58	500	213	50,1050	34	1.1	0302
Arp 220	15 34 57.1	23 30 11	5430	118	5220,5700	10	1.1	0601
NGC 6000	15 49 49.6	-29 23 11	2200	59	1970,2400	25	1.1	0601
NGC 6946	20 34 52.4	60 09 14	50	128	-170,300	11	1.1	0601
NGC 7331	22 37 04.0	34 24 56	820	82	600,1070	14	1.1	0601
					330,1070	12	1.1	0302

a) Source names in italics: previously detected sources; bold-faced: newly detected sources

b) Flux densities are taken from the IRAS Point Source Catalog (Fullmer & Lonsdale 1989)

c) Month (first two digits) and year (last two digits)

d) IC 10: see Henkel et al. (1986); NGC 253: Ho et al. (1987); NGC 1068: Claussen et al. (1984); IC 342: Tarchi et al. (2002a) and Sect. 3.5; NGC 2146: Tarchi et al. (2002b) and Sect. 3.5; NGC 3034 (M 82): Claussen et al. (1984); NGC 3079: Henkel et al. (1984), Haschick & Baan (1985); NGC 3556 and Arp 299: this paper; NGC 5194 (M 51): Ho et al. (1987)

ternative nomenclature, see Sect. 4.2.3), that are separated by 22'' in east-west direction (e.g. Sargent & Scoville 1991). A FIR luminosity of several $10^{11} L_{\odot}$ (Casoli et al. 1992) places Arp 299 near the boundary between luminous (LIRGs) and ultraluminous (ULIRGs) infrared galaxies. Supporting the merging scenario, two highly extended H I tails have been identified by Hibbard & Yun (1999). Radio and infrared observations reveal three main regions of activity (e.g. Gehrzt et al. 1983; Aalto et al. 1997; Casoli et

al. 1999), the nuclear regions of IC 694 and NGC 3690 and an interface where IC 694 and NGC 3690 overlap. NGC 3690 contains a deeply enshrouded active galactic nucleus (AGN), while the situation with respect to the similarly obscured nuclear region of IC 694 is less clear (e.g. Della Ceca et al. 2002; Ballo et al. 2004; Gallais et al. 2004). ¹²CO and HCN $J=1-0$ emission line peaks are strongest toward these most active regions, indicating the presence of large amounts of molecular gas. The positions

Table 3. Line parameters of newly detected masers

Source	Adopted Distance (Mpc)	Epoch (2002)	$\int SdV^a)$ (mJy km s ⁻¹)	$V_{\text{LSR,opt}}^{a,b)}$ (km s ⁻¹)	$\Delta V_{1/2}^a)$ (km s ⁻¹)	Channel Width ^{c)} (km s ⁻¹)	rms (mJy)	$\log L_{\text{H}_2\text{O}}^{d)}$ (L _⊙)	Comments
Mrk 1066	48	Mar 07	696±61	3547.2±1.4	38.7±04.6	1.08	5.3	1.6	see Fig. 1
			169±12	3635.9±0.1	2.1±00.2	1.08	5.3	1.0	see Fig. 1
			171±17	3635.9±0.1	1.9±00.2	0.07	29.7	1.0	see Fig. 2
		Mar 10	822±59	3547.8±1.3	38.3±03.4	1.08	5.6	1.6	see Fig. 1
			193±13	3636.2±0.1	2.1±00.2	1.08	5.6	1.0	see Fig. 1
			157±16	3636.1±0.1	1.2±00.2	0.07	34.9	0.9	see Fig. 2
		May 03	566±16	3552.8±7.7	46.2±16.9	1.08	15.0	1.5	see Fig. 1
			166±33	3635.9±0.2	1.7±00.4	1.08	15.0	0.9	see Fig. 1
		Sep 27	143±31	3635.2±0.2	2.0±00.5	1.08	13.7	0.9	see Fig. 1
Mrk 34 ^{e)}	205	Mar 08	46±14	14661.2±0.4	2.1±00.8	1.16	5.8	1.6	see Fig. 3
			354±52	14837.6±2.3	31.9±05.3	1.16	5.8	2.5	see Fig. 3
			417±78	15771.7±8.7	88.2±16.2	9.29	1.9	2.6	see Fig. 4
		Mar 17	335±57	14840.5±2.9	36.5±07.8	1.16	5.5	2.5	see Fig. 3
			77±24	14674.9±0.8	5.0±01.9	1.16	6.6	1.9	see Fig. 3
		May 07	323±62	14838.7±2.9	31.2±07.6	1.16	6.6	2.5	see Fig. 3
			995±122	15754.9±8.0	130.4±18.4	9.30	2.3	3.0	see Fig. 4
			67±25	14658.2±0.8	4.7±02.2	4.67	3.4	1.8	see Fig. 3
			559±81	14837.4±3.1	43.9±08.2	4.67	3.4	2.7	see Fig. 3
			607±92	15787.2±9.6	115.5±19.9	18.67	1.4	2.8	see Fig. 4
			117±32	15738.2±1.1	6.9±03.0	4.67	3.2	2.1	see Fig. 4
			394±87	15803.1±4.2	47.8±15.0	4.67	3.2	2.6	see Fig. 4
NGC 3556	12	Mar 12	505±72	738.5±1.1	15.1±2.2	1.06	11.6	0.2	see Fig. 5
		Mar 15	99±29	738.0±0.3	2.1±0.5	1.06	10.1	-0.5	see Fig. 5
			421±78	740.3±1.6	17.9±4.8	1.06	10.1	0.1	see Fig. 5
		May 05	229±35	737.2±0.4	4.8±0.8	1.06	10.9	-0.1	see Fig. 5
		Sep 27	329±75	737.1±1.1	10.0±2.9	4.21	6.5	0.0	see Fig. 5
Arp 299	42	Mar 16	6210±242	3101.8±05.1	260.2±11.5	4.30	4.8	2.4	see Fig. 6

a) Obtained from Gaussian fits

b) See the caption to Fig. 1

c) Channel width of the spectra used for the Gaussian fits. Some of the spectra shown in Figs. 1–7 are smoothed

d) $L_{\text{H}_2\text{O}}/[L_{\odot}] = 0.023 \times \int SdV/[\text{Jy km s}^{-1}] \times D^2/[\text{Mpc}^2]$ e) To the observations of the high velocity feature (15787 km s⁻¹) from May 9: The first Gaussian fit refers to the smoothed profile shown in Fig. 4; the latter two component fit refers to the unsmoothed spectrum with a channel spacing of 4.7 km s⁻¹

of strongest ¹³CO $J=1-0$ line emission are, however, displaced from these hotspots (Aalto et al. 1997).

In Arp 299, water maser profiles are extremely broad (~ 200 km s⁻¹), with peak flux densities of 30 mJy (Fig. 6). Adopting a distance of 42 Mpc, the total isotropic luminosity is $\sim 250 L_{\odot}$, placing the object among the more luminous H₂O megamaser sources. The maser line is centered at a velocity of 3100 km s⁻¹, i.e. close to the systemic velocity of the entire complex of sources constituting Arp 299.

3.5. IC 342 and NGC 2146

We also observed the previously detected H₂O maser sources IC 342 and NGC 2146. IC 342 was not detected in June 2001 and March 2002, indicating that the flaring component observed at $V_{\text{LSR}} \sim 16$ km s⁻¹ (Tarchi et al. 2002a) has been quiescent since June 2001. Spectra from NGC 2146, obtained in March 2002, show no significant variations with respect to profiles observed two years earlier (see Tarchi et al. 2002b).

4. Discussion

As indicated in Sect. 1, the surveys presented here have been targeted to detect two classes of extragalactic water masers, ‘jet-masers’ and ‘FIR-masers’.

4.1. The jet-maser sample

Jet-masers provide insight into the interaction of nuclear jets with dense warm molecular gas in the central parsecs of galaxies. All jet-masers known to date arise from the innermost regions of active galaxies and yield important information about the evolution of jets and their hotspots. If continuum emission from the core of the radio source is responsible for variations in maser intensity, monitoring of continuum and line emission can provide estimates, through reverberation mapping, of the speed of the material in the jet, particularly in sources where the jet appears to lie close to the plane of the sky. If, on the other hand, the continuum flare is caused by the brightening of the hotspot or working surface in the jet as it impacts a denser molecular cloud, then the onset of the continuum and maser flares should be nearly simultaneous (Peck et al. 2003).

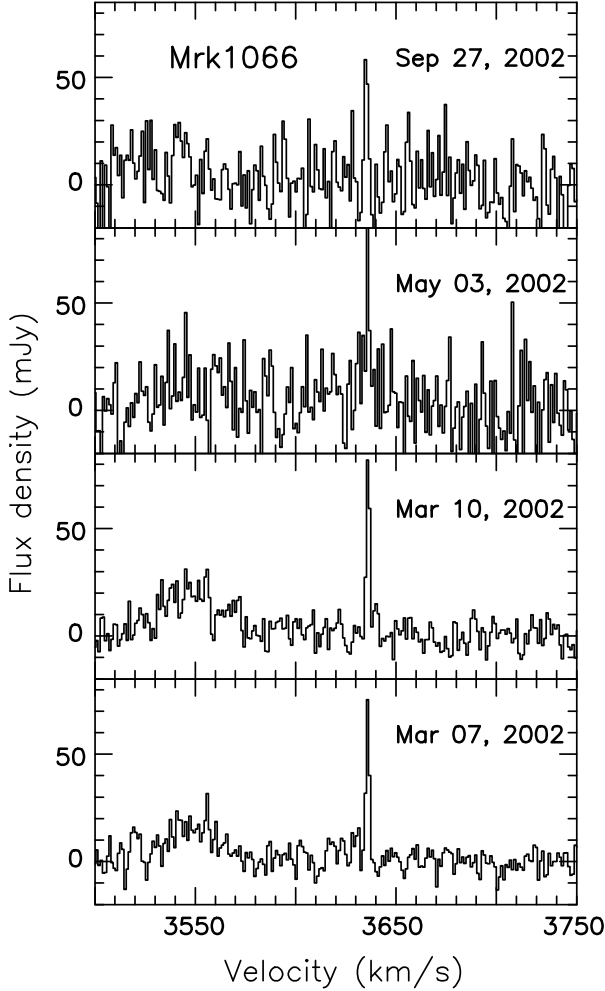


Fig. 1. 22 GHz H₂O megamaser profiles toward Mrk 1066 with a channel spacing of 1.08 km s^{-1} . $\alpha_{2000} = 02^{\text{h}} 59^{\text{m}} 58^{\text{s}}.6$, $\delta_{2000} = 36^{\circ} 49' 14''$. Velocity scales are with respect to the Local Standard of Rest (LSR) and use the optical convention that is equivalent to cz . $V_{\text{sys}} = cz_{\text{sys}} = 3605 \text{ km s}^{-1}$ (NASA/IPAC Extragalactic Database (NED)). $V_{\text{LSR}} - V_{\text{HEL}} = -3.55 \text{ km s}^{-1}$.

In view of these implications we need to investigate the true nature of the megamasers detected in Mrk 1066 and Mrk 34. Are these really jet-masers as suggested by the selection criteria (Sect. 1)? While only VLBI observations can provide a definite answer, a detailed look at well studied jet-masers and the maser sources recently discovered by Braatz et al. (2004) can provide relevant information.

The four jet-maser sources known prior to this survey are NGC 1068 (Gallimore et al. 1996), the Circinus galaxy (Greenhill et al. 2001, 2003a), NGC 1052 (Claussen et al. 1998) and Mrk 348 (Peck et al. 2003). The first two sources show both maser emission from a circumnuclear disk *and* emission arising along the edges of an ionization cone or outflow in the jet. In NGC 1068, the jet-maser velocities are blue-shifted by $\sim 160 \text{ km s}^{-1}$ from systemic and the feature is broad (FWHP (full width to half power) linewidth $\sim 60 \text{ km s}^{-1}$; e.g. Gallimore et al. 2001). In Circinus, both red- and blue-shifted features are seen at

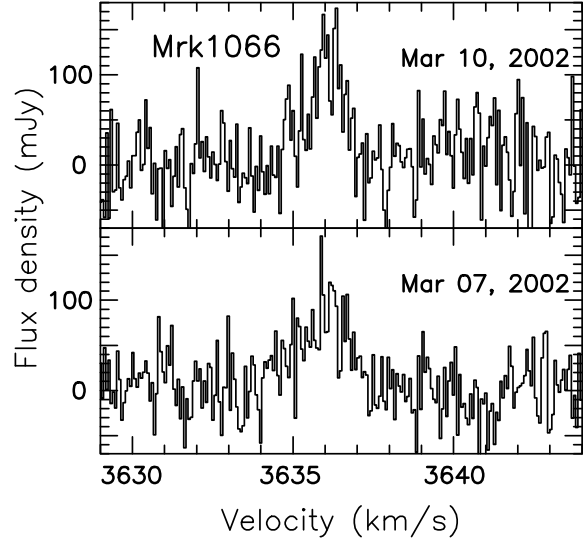


Fig. 2. High spectral resolution profiles of the narrow maser spike in Mrk 1066 (see Fig. 1). The channel spacing is 0.067 km s^{-1} .

velocities up to 160 km s^{-1} from systemic (Greenhill et al. 2003a). In NGC 1052 and Mrk 348, all the maser emission may arise along the jet (Claussen et al. 1998; Peck et al. 2003). As in NGC 1068, this is accompanied by relatively large linewidths (~ 90 and $\sim 130 \text{ km s}^{-1}$) and significant shifts relative to the systemic velocity ($\sim +150$ – 200 and $+130 \text{ km s}^{-1}$), respectively.

To summarize, jet-maser features tend to be broader (a few 10 km s^{-1}) than those typically seen in disk-maser sources like NGC 4258 (a few km s^{-1}) and are usually displaced from the systemic velocity. In Mrk 1066, it is the component at $cz \sim 3550 \text{ km s}^{-1}$ that shows the properties expected in the case of a nuclear jet-type H₂O maser (see Fig. 1). The intense narrow spike near the systemic velocity would have a different origin. We also note, however, that the broad blue- and the narrow red-shifted features bracket the systemic velocity (3605 km s^{-1}). Thus a maser disk like in NGC 4258 cannot be excluded.

Toward Mrk 34, the main components at $cz \sim 14840$ and 15770 km s^{-1} are wide enough for characteristic jet-maser emission. However, the intrinsic weakness of the features requires smoothing which could hide individual narrow components that might represent a significant fraction of the maser emission. Furthermore, Figs. 3 and 4 show two or three velocity components that bracket the systemic velocity ($V_{\text{sys}} = 15145 \pm 90 \text{ km s}^{-1}$; de Grijp et al. 1992). The velocity displacements may not be symmetric; the red-shifted emission (Fig. 4) appears to show a larger displacement than the blue-shifted emission (Fig. 3) from systemic, which would argue against the possibility of a circumnuclear disk. However, the uncertainty in cz_{sys} is large so that an accretion ‘disk-maser’ scenario is also possible. Among the three ‘jet-maser’ sources de-

tected by Braatz et al. (2004; see also Table 1), Mrk 1157 (NGC 591), Mrk 3 and NGC 4151, the first one also shows a profile reminiscent of a disk-maser source. We thus conclude that our jet-maser sample does not provide exclusively jet-maser sources. Having selected sources with jets that appear to be oriented close to the plane of the sky (Sect. 1), this is apparently also an excellent selection criterion to find disk-masers that are characterized by nuclear disks viewed edge-on. Disk-masers may constitute a significant fraction of the newly discovered ‘jet-maser’ sources and some of these may even show both signatures (like NGC 1068) of nuclear activity.

Including all sources that fulfill the selection criteria of our jet-maser sample (Table 1), the detection rate becomes an (almost incredible) 7/14 or 50%. This is the first survey undertaken to look specifically for jet-masers. The number of sources and detections is still too small for a detailed statistical analysis. While it remains to be seen whether the masers are jet- or disk-masers, the unprecedented success rate suggests that both types of masers have been found and that a tilt of $>55^\circ$ between nuclear and large scale disk is a highly favorable configuration for the occurrence of H₂O masers in Seyfert galaxies.

4.2. The FIR-maser sample

4.2.1. Previously detected masers

FIR emission commonly arises from dust grains heated by newly formed stars. In the Milky Way, 22 GHz H₂O masers are associated with sites of (mostly massive) star formation. Therefore our sample of FIR bright galaxies (Table 2) is a suitable tool to detect extragalactic H₂O masers associated with young massive stars. Such masers have the potential to pinpoint the location of prominent star forming regions and to estimate their distance through complementary measurements of proper motion and radial velocity (e.g. Greenhill et al. 1993). Monitoring such masers and determining their three dimensional velocity vectors allows us to derive the gravitational potential of galaxies or groups of galaxies and to improve our understanding of the evolution of such groups with time (for the Local Group, see Brunthaler et al. 2002).

Including the early part of our survey (Tarchi et al. 2002a,b), we detected with IC 342, NGC 2146, NGC 3556 and Arp 299 four new H₂O masers in a total of 45 sources (see Table 2). The new detections are a consequence of higher sensitivity (1σ noise levels of ~ 10 mJy for a 1 km s^{-1} channel), highly improved baselines and luck (in the case of the short-lived flare observed toward IC 342). Including all previously detected sources in the complete sample shown in Table 2, we find a detection rate of 10/45 or $22 \pm 7\%$. For sources with $100 \mu\text{m}$ fluxes in excess of 100 Jy , the detection rate becomes even higher: 7/19 or $37 \pm 14\%$. Detection rates for the jet-maser and the FIR-maser samples lie far above the corresponding rates deduced from other carefully selected samples (see

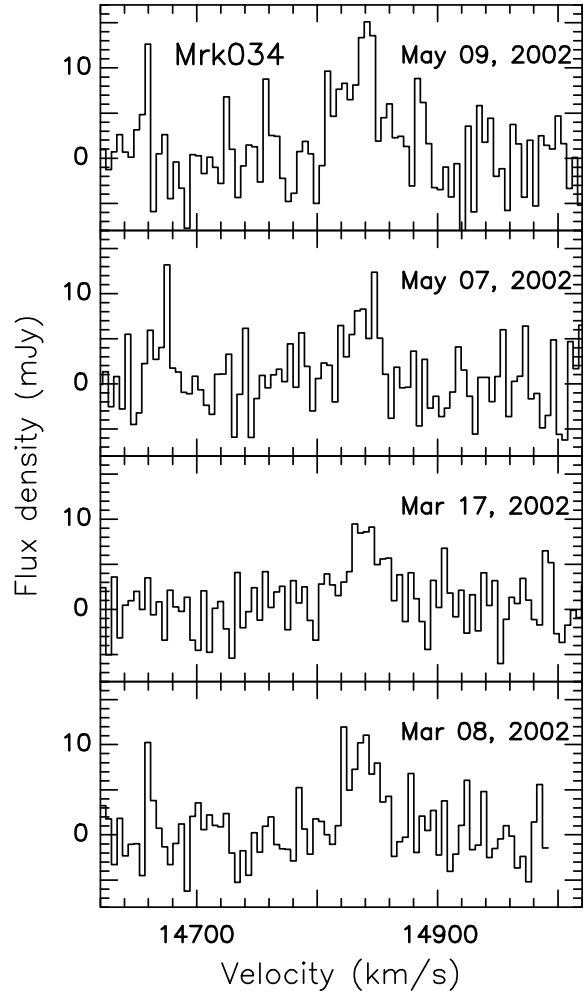


Fig. 3. Low velocity H₂O megamaser profiles toward Mrk 34 with a channel spacing of 4.65 km s^{-1} . $\alpha_{2000} = 10^{\text{h}} 34^{\text{m}} 08^{\text{s}}.6$, $\delta_{2000} = 60^\circ 01' 52''$. $c z_{\text{sys}} = 15145 \text{ km s}^{-1}$ (de Grijs et al. 1992). $V_{\text{LSR}} - V_{\text{HEL}} = +5.23 \text{ km s}^{-1}$.

e.g. Henkel et al. 1984, 1986, 1998; Haschick & Baan 1985; Braatz et al. 1996; Greenhill et al. 2002).

To find out why the FIR-maser sample contains numerous 22 GHz H₂O maser sources and to elucidate the nature of the sources in NGC 3556 and Arp 299, we have to classify the properties of the previously studied masers of this sample. Two of the sources, those in NGC 1068 and NGC 3079, are luminous megamasers (e.g. Gallimore et al. 2001; Trotter et al. 1998). The weaker ‘kilomasers’ in IC 10, IC 342, NGC 2146 and NGC 3034 (M 82) are associated with sites of massive star formation (Argon et al. 1994; Baudry & Brouillet 1996; Tarchi et al. 2002a,b). There are also two known weak nuclear kilomasers, in NGC 5194 (M 51) (Hagiwara et al. 2001b) and in NGC 253 (Henkel et al. 2004). Whether they are related to the nearby AGN or to star formation remains, however, unclear.

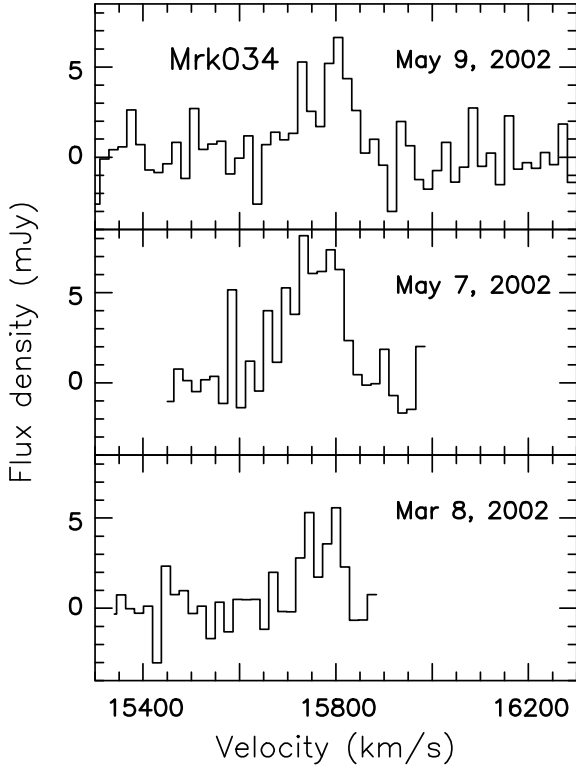


Fig. 4. High velocity megamaser feature toward Mrk 34 with a channel spacing of 18.65 km s^{-1} .

4.2.2. NGC 3556

The position of the H₂O kilomaser in NGC 3556 is not yet accurately known. From the relative number of nuclear versus non-nuclear masers of similar luminosity, the most likely interpretation is an association with a site of massive star formation. In view of NGC 253 and NGC 5194, however, there is a small chance for a nuclear maser in NGC 3556.

4.2.3. Arp 299

As indicated in Sect. 3.4, the merging system Arp 299 is composed of two galaxies, NGC 3690 in the west, IC 694 in the east, and a star-bursting interface or overlap region $10''$ north of NGC 3690¹. Since NGC 3690 and IC 694 are only half a beam size ($20''$) apart in our observations and since the separation between NGC 3690 and the overlap region is even smaller, extremely good pointing conditions were needed to map the region. Three maps were made. Fig. 7 shows the most accurate (pointing accuracy $\pm 4''$)

¹ According to NED, the entire merger forms NGC 3690, while IC 694 is a less prominent galaxy $\sim 1'$ to the northwest. The latter target was observed by Braatz et al. (2004) in the H₂O line. A 1σ noise limit of 2.4 mJy per 0.3 km s^{-1} channel was obtained. Here we follow the more traditional nomenclature that is commonly used in the literature.

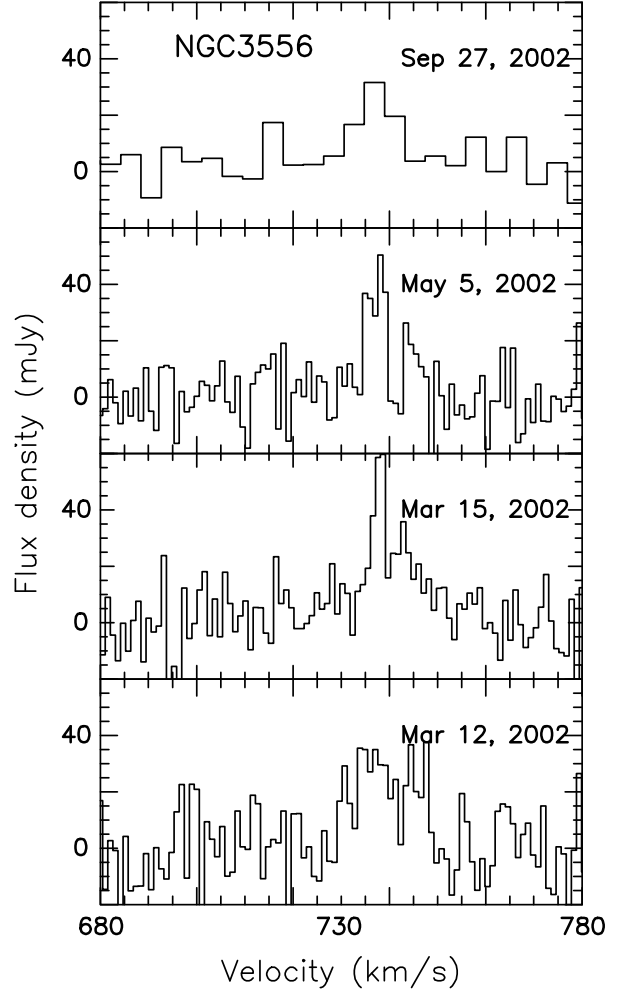


Fig. 5. H₂O kilomaser spectra toward NGC 3556 ($\alpha_{2000} = 11^{\text{h}} 11^{\text{m}} 31^{\text{s}}.2$, $\delta_{2000} = 55^{\circ} 40' 25''$). Channel spacings are 4.2 km s^{-1} (upper panel) and 1.06 km s^{-1} . $cz = 700 \text{ km s}^{-1}$ (NED). $V_{\text{LSR}} - V_{\text{HEL}} = +5.90 \text{ km s}^{-1}$.

and extended, albeit also the most noisy one. In spite of the rather low signal-to-noise ratios we note that (1) H₂O emission may originate from more than one hotspot; (2) one of the potential sources, the one in the east, is close to IC 694, where an OH megamaser was already reported (Baan & Haschick 1990); (3) there appears to be a western peak of emission that is located near the center of the second dominant galaxy of the system, NGC 3690; (4) a broader feature near the center is likely caused by blending of the two main hotspots associated with IC 694 and NGC 3690; (5) the vigorously star forming overlap region appears to be devoid of H₂O megamaser emission.

When we compare these results with the CO velocity field observed by Casoli et al. (1999), we find that the H₂O velocity of the eastern peak, 2980 km s^{-1} , is consistent with the CO velocity of the south-eastern part of IC 694 (i.e. offset w.r.t. the nucleus of IC 694 that has a velocity of $cz = 3110 \text{ km s}^{-1}$). Although the location of the western hotspot is close to the core of NGC 3690, the velocities of the maser emission, the CO

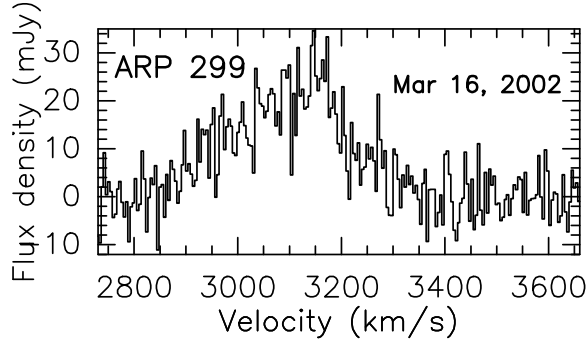


Fig. 6. H₂O megamaser profile toward Arp 299 ($\alpha_{2000} = 11^{\text{h}} 28^{\text{m}} 31^{\text{s}}.9$, $\delta_{2000} = 58^{\circ} 33' 45''$). The channel spacing is 4.3 km s^{-1} . $V_{\text{LSR}} - V_{\text{HEL}} = +6.97 \text{ km s}^{-1}$. For radial velocities, see Sect. 4.2.3.

lines and the systemic velocity of NGC 3690 do not match perfectly ($\sim 3100 \text{ km s}^{-1}$ from CO, $c_{z_{\text{sys}}} = 3121 \text{ km s}^{-1}$ (NASA/IPAC Extragalactic Database (NED)), versus $\sim 3150 \text{ km s}^{-1}$ from H₂O). Interestingly, velocities near 3150 km s^{-1} as seen in H₂O are consistent with those of the overlap region.

A comparison of the profile shown in Fig. 6 with the central one in Fig. 7 suggests a slight offset in position (a few arcsec in east-west direction) and weaker peak emission in the latter case. This is within the uncertainties of pointing and calibration, but maser variability can also explain the differences.

With the H₂O emission likely originating from IC 694 and NGC 3690, Arp 299 is the fourth extragalactic system beyond the Magellanic Clouds that is known to exhibit $\lambda = 18 \text{ cm}$ OH and $\lambda = 1.3 \text{ cm}$ H₂O maser emission (in NGC 253, NGC 1068 and M 82, such masers are also observed; see Weliachew et al. 1984; Turner 1985; Baudry & Brouillet 1996; Gallimore et al. 1996; Henkel et al. 2004). In these other galaxies, however, either H₂O or OH or both lines only reach kilomaser luminosities. IC 694 may thus be the first known galaxy with both an OH and an H₂O megamaser (for OH, see Baan & Haschick 1990). The global OH and H₂O line profiles appear to be similar, except for a weak OH feature at $\sim 3500 \text{ km s}^{-1}$ that is not seen in H₂O.

Arp 299 is the second most luminous FIR source with a known H₂O megamaser. While OH megamasers are closely associated with ultraluminous infrared galaxies (ULIRGs; see e.g. Darling & Giovanelli 2002a), the only ULIRG with a luminous H₂O maser was so far NGC 6240 (Hagiwara et al. 2002, 2003a; Nakai et al. 2002; Braatz et al. 2003). In accordance with the observed anticorrelation between the occurrence of OH and H₂O megamasers (OH megamasers may arise from low density molecular gas, while H₂O megamasers originate from gas of much higher density; e.g. Kylafis et al. 1991; Randell et al. 1995), this is one of those ULIRGs in which no OH emission is seen. The second detection of an H₂O megamaser in a luminous

FIR galaxy (although Arp 299 is not quite as luminous as NGC 6240) makes a dedicated survey of such luminous FIR galaxies worthwhile.

4.2.4. Detection probabilities

The high rate of maser detections in our sample of FIR luminous galaxies (Table 2) strongly suggests that a relationship between FIR flux density and maser phenomena exists, consistent with the assessment of HWB. The detection rate for masers in accretion disks is dictated by tight geometric constraints. The cumulative maser output of a star forming region may not be so narrowly confined.

Fig. 8 shows the cumulative detection rate above a given $100 \mu\text{m}$ IRAS Point Source Catalog flux for the parent galaxy. The detection rate strongly declines with decreasing FIR flux. For fluxes $\sim 1000 \text{ Jy}$, $100\text{--}300 \text{ Jy}$, and $50\text{--}100 \text{ Jy}$, we find detection rates of 2/2 or 100%, 5/17 or 29% and 3/26 or 12% (unlike in Fig. 8, these are not cumulative detection rates but detection rates related to their specific FIR flux density interval). Maffei 2 and NGC 5236 (M 83) show no detectable maser emission near their nuclei but have $S_{100 \mu\text{m}} > 200 \text{ Jy}$. In view of the statistical properties of the sample, frequent monitoring of these sources would likely reveal H₂O maser emission, possibly a short-lived flare like that seen in IC 342 (Tarchi et al. 2002a).

Fig. 8 shows a detection probability of $\sim 50\%$ for sources with $S_{100 \mu\text{m}} \gtrsim 120 \text{ Jy}$. If the two brightest FIR sources, NGC 253 and M 82 (NGC 3034), were at $D \sim 10 \text{ Mpc}$ (i.e. three times their estimated distance), this would imply $S_{100 \mu\text{m}} \sim 100 \text{ Jy}$ and H₂O peak fluxes of $\sim 5 \text{ mJy}$ (broad emission feature) and $\sim 10 \text{ mJy}$ (narrow emission feature), respectively (for the line profiles, see Ho et al. 1987; Baudry et al. 1994; Henkel et al. 2004). Thus the two sources would be just below the detection limit, consistent with the detection probability at the corresponding $100 \mu\text{m}$ flux.

While there is significant scatter (among the sources of Table 2, the most extreme source by far is NGC 3079, whose H₂O maser would be detectable even at a distance corresponding to $S_{100 \mu\text{m}} \sim 10 \text{ Jy}$), we conclude that at present sensitivities, there is for most sources a detection threshold near $S_{100 \mu\text{m}} = 100 \text{ Jy}$. It appears that $S_{100 \mu\text{m}}$ and H₂O peak fluxes are roughly proportional, as was already suggested by HWB on the basis of a smaller number of detected sources. Such a result is reminiscent of the $L_{\text{FIR}} - L_{\text{H}_2\text{O}}$ correlation found by Jaffe et al. (1981) for galactic star forming regions and is readily explained if most of the detected sources in our FIR sample are associated with sites of massive star formation. Four of the ten detected sources are indeed related to star formation, two to AGN, while the nature of the remaining four is uncertain. While the scatter is large, nevertheless even the AGN related megamaser galaxies roughly follow the correlation found for galactic sources, i.e. $L_{\text{FIR}}/L_{\text{H}_2\text{O}} \sim 10^9$ (see Fig. 9). This is difficult to explain and might be caused by

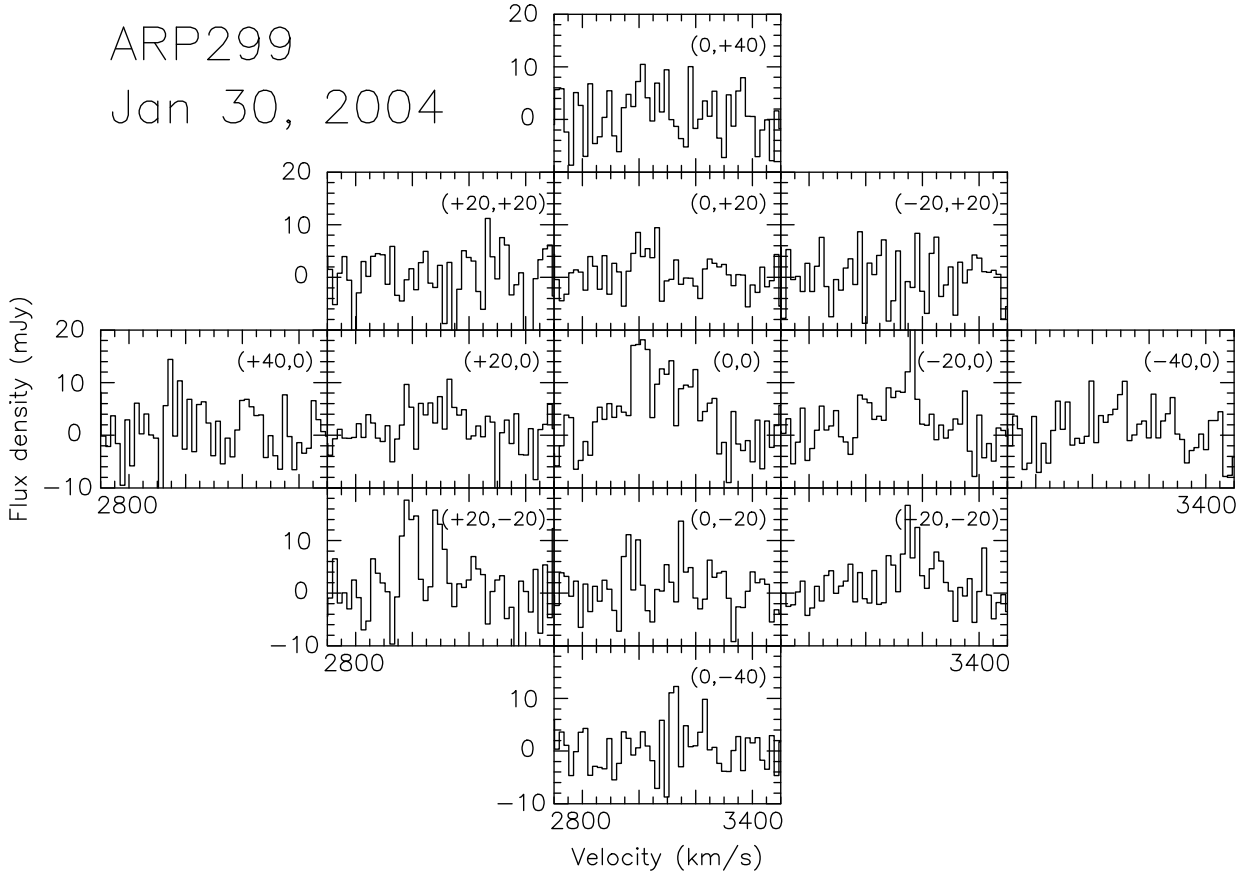


Fig. 7. H₂O megamaser profiles toward Arp 299, taken on Jan 30, 2004, during a night with excellent pointing conditions. The reference position is $\alpha_{2000} = 11^{\text{h}} 28^{\text{m}} 31^{\text{s}}.9$, $\delta_{2000} = 58^{\circ} 33' 45''$. Offsets in arcsec ($\Delta\alpha$, $\Delta\delta$) are given in the upper right corner of each box. Spectra with offsets $\Delta\alpha = -20''$ trace emission from the ‘overlap’ region (north) and NGC 3690 (south). Spectra with $\Delta\alpha = +20''$ are sensitive to emission from IC 694 (see Sect. 4.2.3). The channel spacing is 16.8 km s^{-1} .

a spatially extended cascade of nuclear bars that contains warm dust and that is needed to fuel the very nuclear region (e.g. Shlosman & Heller 2002).

Given the correlation between FIR and H₂O maser flux densities, an improvement in sensitivity by one order of magnitude to detect H₂O masers would lower the $100 \mu\text{m}$ flux threshold from $\sim 100 \text{ Jy}$ to $\sim 10 \text{ Jy}$, and would provide a ~ 25 times richer sample of detectable targets (~ 250 sources at $\delta > -30^\circ$). This enlarged sample might then also include some of the brighter ULIRGs that are not part of this study because of too large distances and correspondingly low infrared flux densities.

4.3. The entire extragalactic maser sample

4.3.1. The distance bias

Table 4 lists the 53 galaxies with a total of 57 groups of H₂O masers detected beyond the Magellanic Clouds. The separation between megamasers (AGN environment) and kilomasers (mainly star formation) is not entirely clear. NGC 2782, an $L_{\text{H}_2\text{O}} \sim 12 L_\odot$ maser, *might* not possess an AGN (e.g. Braatz et al. 2004), while the masers in NGC 2146 (a total of $\sim 8 L_\odot$; see Table 5) are known to be related to star formation (Tarchi et al. 2002b). A clear separation between jet and accretion disk masers would also

be appropriate. The lack of high resolution data toward most sources, however, makes such a classification elusive. We thus group the masers according to their isotropic luminosity, assuming that all sources with $L_{\text{H}_2\text{O}} \geq 10 L_\odot$ (the megamasers) are nuclear.

The H₂O detections presented in Table 4 were collected from various surveys with different sensitivities and even within a survey, noise levels may differ from source to source. Furthermore, the masers are time variable and it is always more difficult to detect a broad weak feature than a stronger but narrower spectral component. In view of this highly heterogeneous data base, we adopt a characteristic linewidth of the dominant spectral feature of 20 km s^{-1} and a detection threshold of 50 mJy (this sensitivity is inferior to that in our surveys (Sects. 4.1 and 4.2) and reflects the higher noise levels of most other data, the exception being the Braatz et al. 2004 survey). We should then be able to detect masers with 1, 10, 100, 1000, and $10000 L_\odot$ out to maximal distances of

$$D/\text{Mpc} = [(L_{\text{H}_2\text{O}}/L_\odot)/(0.023 \times S/\text{Jy} \times \Delta V/\text{km s}^{-1})]^{1/2},$$

i.e. 6.5, 21, 65, 210, and 650 Mpc, respectively. Note that these distance limits only depend on the square root of the adopted observational sensitivity.

We can check how consistent this is with the sample of detected masers listed in Table 4. The total H₂O lu-

Table 4. Extragalactic H₂O masers beyond the Magellanic Clouds

Source	R.A. (J2000)	Dec.	V_{sys} (cz)	D (Mpc)	$\log L_{\text{FIR}}^{\text{a})}$ (log L _⊙)	$T_{\text{dust}}^{\text{a})}$ (K)	$\log L_{\text{H}_2\text{O}}^{\text{a})}$ (log L _⊙)	Ref. ^{b)}
IC 10	00 20 17.9	+59 18 31	−350	1.2	8.2	40	−1.7	1
	00 20 27.0	+59 17 29					−0.8	2,3
NGC 253	00 47 33.1	−25 17 17	240	3.0	10.3	52	−0.8	4,5
	00 47 33.6	−25 17 14					−1.7	5
NGC 262 (Mrk348)	00 48 47.1	+31 57 25	4505	62.0	10.6	42	2.6	6,7
IRAS F0106–8034	01 07 00.9	−80 18 24	5045	67.0	10.7	32	2.7	8
NGC 449 (Mrk 1)	01 16 07.2	+33 05 22	4780	64.0	10.6	55	1.7	9
NGC 598 (M 33)	01 33 16.5	+30 52 50	−180	0.7	9.0	36	−0.5	10,11
	01 33 29.4	+30 31 55					−1.5	12
NGC 591 (Mrk 1157)	01 33 31.2	+35 40 06	4555	61.0	10.5	46	1.4	13
NGC 1052	02 41 04.8	−08 15 21	1470	17.0	9.1	54	2.1	9,14
NGC 1068	02 42 40.7	−00 00 48	1135	14.5	11.2	54	2.2	15,16
Mrk 1066	02 59 58.6	+36 49 14	3600	48.0	10.9	55	1.5	13,17
NGC 1386	03 36 46.4	−36 00 02	870	17.0	9.8	46	2.1	18
IC 342 ^{c)}	03 46 46.3	+68 05 46	40	2.0	9.0	49	−2.0	19
UGC 3255	05 09 50.2	+07 29 00	5675	75.0	10.5	40	1.2	13
Mrk 3	06 15 36.3	+71 02 15	4010	54.0	10.7	69	1.0	13
NGC 2146	06 18 36.6	+78 21 28	900	14.5	10.9	53	0.0	20
	06 18 38.6	+78 21 24					0.0	20
Mrk 78	07 42 41.7	+65 10 37	11195	150.0	11.0	60	1.5	13
Mrk 1210	08 04 05.8	+05 06 50	4045	54.0	10.5	75	1.9	9
NGC 2639	08 43 38.1	+50 12 20	3335	44.0	10.4	34	1.4	9,21
NGC 2782	09 14 05.1	+40 06 49	2560	34.0	10.5	47	1.1	13
NGC 2824 (Mrk 394)	09 19 02.2	+26 16 12	2760	37.0	9.7	47	2.7	22
NGC 2960 (Mrk 1419)	09 40 36.4	+03 34 37	4930	66.0	10.5	38	2.6	23
NGC 2979	09 43 08.5	−10 23 01	2720	36.0	9.9	38	2.1	22
NGC 3034 (M 82)	09 55 52.2	+69 40 47	200	3.7	10.6	65	0.0	15,24
NGC 3079	10 01 57.8	+55 40 47	1120	15.5	10.6	42	2.7	25,26,27
IC 2560	10 16 18.7	−33 33 50	2925	35.0	10.2	47	2.0	18,28
Mrk 34	10 34 08.6	+60 01 52	15140	205.0	11.2	55	3.0	17
NGC 3556	11 11 31.2	+55 40 25	700	12.0	10.5	38	0.0	17
Arp 299 (Mrk 171)	11 28 32.2	+58 33 44	3120	42.0	11.7	61	2.1	17
NGC 3735	11 35 57.3	+70 32 09	2695	36.0	10.6	38	1.3	29
NGC 4051	12 03 09.6	+44 31 53	730	10.0	9.6	38	0.3	30
NGC 4151	12 10 32.6	+39 24 21	1000	13.5	−0.2	13
NGC 4258	12 18 57.5	+47 18 14	450	7.2	9.9	33	1.9	15,31
NGC 4388	12 25 46.7	+12 39 44	2520	34.0	10.7	47	1.1	13
ESO 269–G012	12 56 40.7	−46 55 31	4950	66.0	3.0	22
NGC 4922	13 01 25.2	+29 18 50	7080	95.0	11.2	61	2.3	13
NGC 4945	13 05 27.5	−49 28 06	560	4.0	10.3	45	1.7	32,33
NGC 5194 (M 51)	13 29 52.7	+47 11 43	450	10.0	10.3	33	−0.2	4,34
NGC 5256 (Mrk 266)	13 38 17.2	+48 16 32	8365	112.0	11.5	46	1.5	13
NGC 5347	13 53 17.8	+33 29 27	2335	31.0	9.9	44	1.5	18
Circinus	14 13 09.3	−65 20 21	450	4.0	10.1	54	1.3	35,36
NGC 5506 (Mrk 1376)	14 13 14.8	−03 12 27	1850	25.0	10.3	59	1.7	9
NGC 5643	14 32 40.7	−44 10 28	1200	16.0	10.3	39	1.4	22
NGC 5728	14 42 23.9	−17 15 11	2795	37.0	10.6	45	1.9	13
NGC 5793	14 59 24.7	−16 41 36	3490	47.0	10.6	47	2.0	37,38
NGC 6240	16 52 58.1	+02 23 50	7340	98.0	11.8	58	1.6	39,40,41,42
NGC 6300	17 17 00.3	−62 49 15	1110	15.0	10.2	36	0.5	22
NGC 6323	17 13 18.0	+43 46 56	7790	104.0	2.7	13
ESO103–G035	18 38 20.3	−65 25 42	3985	53.0	10.5	121	2.6	18
IRAS F19370–0131	19 39 38.9	−01 24 33	6000	80.0	10.7	59	2.2	22
3C403	19 52 15.8	+02 30 24	17690	235.0	11.2	...	3.3	43
NGC 6926	20 31 38.7	−80 49 58	5970	80.0	11.1	39	2.7	22
TXS2226–184	22 29 12.5	−18 10 47	7495	100.0	3.8	44
IC 1481	23 19 25.1	+05 54 21	6120	82.0	10.4	65	2.5	18

a) For the determination of L_{FIR} and T_{dust} (60/100 μm color temperatures), see Wouterloot & Walmsley (1986). The IRAS fluxes were taken from Fullmer & Lonsdale (1989) and, for a few sources (NGC 598, NGC 4258, IRAS F19370–1031 and 3C403), from NED. While, as already noted by HWB and Braatz et al. (1997), the derived dust temperatures are mostly well above 30 K and thus rather large, a correlation between T_{dust} and $L_{\text{H}_2\text{O}}$ is not apparent.

b) References: (1) Henkel et al. (1986) (2) Becker et al. (1993) (3) Argon et al. (1994) (4) Ho et al. (1987) (5) Henkel et al. (2004) (6) Falcke et al. (2000) (7) Peck et al. (2003) (8) Greenhill et al. (2002) (9) Braatz et al. (1994) (10) Churchwell et al. (1977) (11) Greenhill et al. (1993) (12) Huchtmeier et al. (1978) (13) Braatz et al. (2004) (14) Claussen et al. (1998) (15) Claussen et al. (1984) (16) Gallimore et al. (2001) (17) This paper (18) Braatz et al. (1996) (19) Tarchi et al. (2002a) (20) Tarchi et al. (2002b) (21) Wilson et al. (1995) (22) Greenhill et al. (2003b) (23) Henkel et al. (2002) (24) Baudry & Brouillet (1996) (25) Henkel et al. (1984) (26) Haschick & Baan (1985) (27) Trotter et al. (1998) (28) Ishihara et al. (2001) (29) Greenhill et al. (1997a) (30) Hagiwara et al. (2003b) (31) Herrnstein et al. (1999) (32) Dos Santos & Lépine (1979) (33) Greenhill et al. (1997b) (34) Hagiwara et al. (2001b) (35) Gardner & Whiteoak (1982) (36) Greenhill et al. (2003a) (37) Hagiwara et al. (1997) (38) Hagiwara et al. (2001a) (39) Hagiwara et al. (2002) (40) Nakai et al. (2002) (41) Braatz et al. (2003) (42) Hagiwara et al. (2003a) (43) Tarchi et al. (2003) (44) Koekemoer et al. (1995)

c) The maser luminosity refers to a brief flaring episode

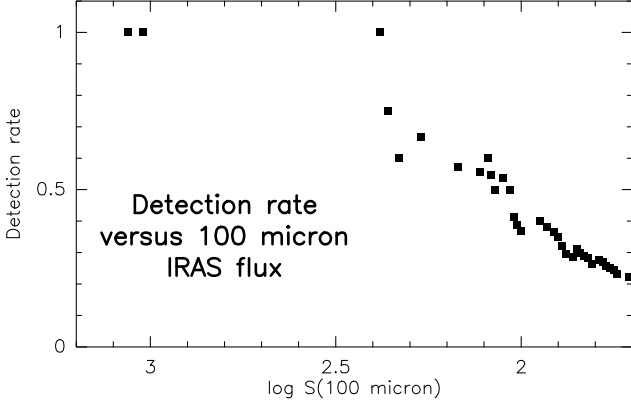


Fig. 8. Detection rate of the H₂O FIR-maser sample (see Table 2 for the targets and Sect. 1 for selection criteria) including all galaxies above a given IRAS Point Source Catalog $S_{100\mu\text{m}}$ flux density.

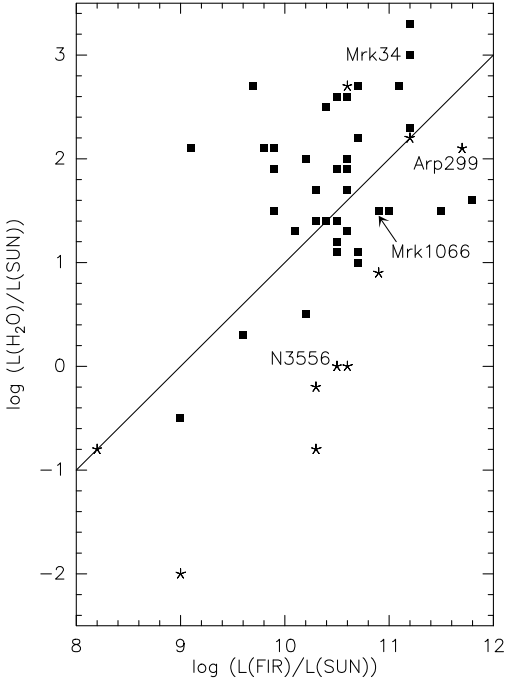


Fig. 9. IRAS Point Source FIR luminosity versus total H₂O luminosity of H₂O detected galaxies (cf. Table 4). For NGC 2146, the total logarithmic H₂O luminosity is 0.9 in solar units (Tarchi et al. 2002a). Stars denote the ten sources belonging to the FIR selected maser sample. The diagonal line shows the correlation found by Jaffe et al. (1981) for individual galactic star forming regions.

minosity per galaxy is taken. Table 5 shows the results. The number of detections in the most likely distance bin is given in italics. IC 342 was not included because of the intrinsic weakness of its maser. It is apparent that for the kilomaser galaxies (here defined to show luminosities $<10L_{\odot}$) either the number of sources in the expected bin is by far the highest or there are additional detections at both lower and higher distances (the latter a conse-

quence of the fact that the sensitivity of the surveys is not uniform). This provides a picture that is approximately consistent with expectations.

For the more luminous megamasers the situation is different. The distance distribution of the 20 masers with $10L_{\odot} \leq L_{\text{H}_2\text{O}} < 100L_{\odot}$ is still consistent. Four are located at $D < 21$ Mpc, and four at a distance higher than the estimated limiting distance of 65 Mpc. Most of the detections are obtained in their most likely distance bin. Among the 18 masers with $100L_{\odot} \leq L_{\text{H}_2\text{O}} < 1000L_{\odot}$, however, 13 are closer or near $D \sim 65$ Mpc, the inner limit of the most likely distance range, while among the four galaxies with $1000L_{\odot} \leq L_{\text{H}_2\text{O}} < 10000L_{\odot}$, three are closer than the corresponding $D \sim 210$ Mpc limit. The fourth megamaser, 3C 403, surpasses this limit by only a small amount. None of the masers in the last two groups has a distance larger than the estimated maximum distance.

The surveys do not cover the entire sky and are therefore incomplete by an unknown amount. The fact that distances of masers with lower luminosity are consistent with expected values indicates that a bias related to the distance of these sources is negligible. Most of the luminous megamasers ($L_{\text{H}_2\text{O}} \geq 100L_{\odot}$), however, are observed at distances that are smaller than expected. Is this an effect of different lineshapes or a consequence of the observed sample of sources? Considering the four most luminous targets with $L_{\text{H}_2\text{O}} \geq 1000L_{\odot}$, only TXS2226–184 has an unusually wide profile, while the others show ‘normal’ lineshapes. Without going into any detail, we note that the situation is similar for sources with $100L_{\odot} \leq L_{\text{H}_2\text{O}} < 1000L_{\odot}$. We thus conclude that the bias towards ‘nearby’ sources in the sample of luminous water masers is caused by the selection of galaxies so far observed. The entire megamaser sample is dominated by the surveys of Braatz et al. (1994, 1996, 1997, 2003, 2004) that are mostly confined to recessional velocities $\lesssim 7000 \text{ km s}^{-1}$, i.e. out to $D \sim 100$ Mpc (this also holds for the two surveys discussed in Sects. 4.1 and 4.2). Sources with significantly larger distances were rarely observed.

From the number of sources at ‘near’ distances we may extrapolate to the larger volumes to estimate the percentage of missing detections in this larger volume. This may provide lower limits because detections at the ‘nearby’ distances may be incomplete as well. For the more luminous megamasers with $100L_{\odot} \leq L_{\text{H}_2\text{O}} < 1000L_{\odot}$, four sources are observed within $D = 21$ Mpc, so that $\sim 4000 \pm 2000$ detectable targets may be expected within $D = 210$ Mpc. This has to be compared with 16 known such objects. With 11 known sources within ~ 65 Mpc, we still expect $\sim 350 \pm 105$ objects within $D = 210$ Mpc, a factor of ~ 20 above the detected number. Among the most luminous four sources, those with $L_{\text{H}_2\text{O}} \gtrsim 1000L_{\odot}$, three are detected inside of 210 Mpc, so we would expect 100 ± 60 detectable targets out to $D = 650$ Mpc, of which so far only four have been identified.

While the large errors in the predicted numbers of detectable sources may raise scepticism, an analysis of the distances of the galaxies belonging to the two most lumi-

Table 5. Number of detected maser galaxies per luminosity and distance interval (see Table 4)^{a)}

$\log(L_{\text{H}_2\text{O}})$ (L_\odot)	Distance (Mpc)					
	<2	2–6	6–21	21–65	65–210	210–650
–1.0–(–0.1)	2	<i>1</i>	2	–	–	–
0.0–0.9	–	1	4	–	–	–
1.0–1.9	–	2	2	<i>12</i>	4	–
2.0–2.9	–	–	4	7	7	–
3.0–3.9	–	–	–	–	3	<i>1</i>

a) In italics: Expected highest distance bin where sources of a given luminosity should still be detectable. Because this distance bin contains a much larger volume than the nearer ones, most masers are expected to be there. For each of the galaxies in Table 4 the total integrated 22 GHz H₂O luminosity was taken. This amounts to an integrated single-dish flux density corresponding to $\sim 8 L_\odot$ in the case of NGC 2146, where VLA data from Tarchi et al. (2002b) revealed two $\sim 1 L_\odot$ masers (see Table 4).

nous H₂O luminosity bins ($100 L_\odot \leq L_{\text{H}_2\text{O}} < 10000 L_\odot$) yields a clear result. 14 of the 22 sources in these bins are not in the expected most distant shell (between $D=65$ and 210 or between $D=210$ and 650 Mpc, respectively) but are located more nearby. Two additional sources are located at the inner boundary of the most likely shell, while no source is detected beyond the estimated distance limit. This implies that the majority of sources, 73%, is located within a volume that encompasses only 3.2% of the volume in which the masers would be detectable. Assuming an isotropic spatial distribution and applying the Bernoulli theorem, a deviation of 8% from 73% corresponds to 1σ . The discrepancy between the expected (3.2% of the detections in the inner, 96.8% in the outer shell) and observed (73% in the inner, 27% in the outer shell) spatial distributions is therefore significant. We conclude that statistical evidence strongly indicates that only *a tiny fraction of the luminous megamaser sources detectable with presently available instrumentation has been discovered to date.*

So far we have not yet considered that the maser luminosities are not necessarily at the upper edge of their respective bin. This has the consequence that not all of them should be detectable out to the upper limit of the corresponding most likely distance interval. To quantify this we have to determine the H₂O luminosity function.

4.3.2. The H₂O maser luminosity function

The luminosity function $\Phi(L_{\text{H}_2\text{O}})$ is the number density of objects with luminosity $L_{\text{H}_2\text{O}}$ per logarithmic interval in $L_{\text{H}_2\text{O}}$. An unbiased direct measurement of $\Phi(L_{\text{H}_2\text{O}})$ would require that all objects with a given luminosity be detected within the survey volume, which is not possible in flux limited surveys like those presented in Sects. 4.1 and 4.2. Instead, each object in a survey has an effective volume in which it could have been detected and the sum of de-

tections weighted by their available volumes V_i determines the luminosity function.

Not accounting for the incompleteness of the detected H₂O megamaser sample and ignoring the possibility that in different luminosity bins the fraction of detected sources may be different, we can derive a zeroth order approximation to the luminosity function (LF) of extragalactic H₂O maser sources. Such a computation is not only limited by the effects mentioned above but there are additional factors, the main three being:

- (a) Non-uniform sky coverage resulting from several large and many small surveys. Most of the large surveys have used optical-magnitude-limited samples of galaxies in the northern sky. We have approximated the sky coverage to be the entire northern sky;
- (b) Different sensitivity limits in the various surveys. We have considered two typical detection thresholds: 1 Jy km s^{-1} (from e.g. a detection limit of a 20 km s^{-1} line with peak flux 50 mJy) and 0.2 Jy km s^{-1} (i.e. five times weaker).
- (c) The use of optical-magnitude limited galaxy samples for H₂O maser surveys. Given this, the H₂O maser LF is best calculated via the optical LF and the bivariate H₂O and optical LF (e.g. Meurs & Wilson 1984). Given the diversity of the selection criteria in different surveys, however, we are forced to directly calculate the H₂O LF.

We use the standard V/V_{max} method (Schmidt 1968) to estimate the H₂O LF. The sample objects (Table 4) were divided into bins of 0.5 dex over the range $L_{\text{H}_2\text{O}} = 10^{-1} - 10^4 L_\odot$. For each luminosity bin (L_p ; $p=1,10$) we calculated the differential LF value as follows:

$$\Phi(L_p) = \frac{4\pi}{\Omega} \sum_{i=1}^{n(L_p)} (1/V_{\text{max}})_i$$

Here $n(L_p)$ is the number of galaxies with $L_p - 0.25 < \log L_{\text{H}_2\text{O}} < L_p + 0.25$. The term after the summation sign represents the inverse of the maximum volume (V_{max}) over which an individual galaxy can be detected given its maser luminosity and the detection limit of the survey. As discussed above in (b), we consider two different detection limits: 0.2 Jy km s^{-1} and 1 Jy km s^{-1} . In the former case, 6 masers have to be left out of the computation since they are weaker than the assumed detection limit, and in the latter case 19 masers have to be omitted. The maser in IC 342 is outside the considered H₂O luminosity range. Results are plotted in Fig. 10 for both detection limits.

Fig. 10 demonstrates that the H₂O luminosity function does not strongly depend on the detection limit used. From the overall slope of the luminosity function we derive $\Phi \propto (\log L_{\text{H}_2\text{O}})^{-1.6}$ which is steeper than the LF for OH megamasers (see Darling & Giovanelli 2002b). Noteworthy is the fast decay in the number of sources at the upper end of the maser luminosity function that could indicate that ultraluminous H₂O ‘gigamasers’ are rare. Obvious is also a low number of sources in the $1-10 L_\odot$ bin. This bin marks the upper end of the luminosity distribution of known star forming regions and is located slightly below the luminosity of the ‘weak’ megamaser sources. So there might exist

a minimum of H₂O emitting targets just below the megamaser luminosity threshold. Both results, the minimum at $L_{\text{H}_2\text{O}} = 1\text{--}10 L_\odot$ and the fast decline at highest maser luminosities, are, however, of questionable significance. The number of sources in the $L_{\text{H}_2\text{O}} = 0.1\text{--}10 L_\odot$ bins is not yet large enough to make a convincing case. And Fig. 10 does not account for the distance bias discussed for the most luminous sources in Sect. 4.3.1.

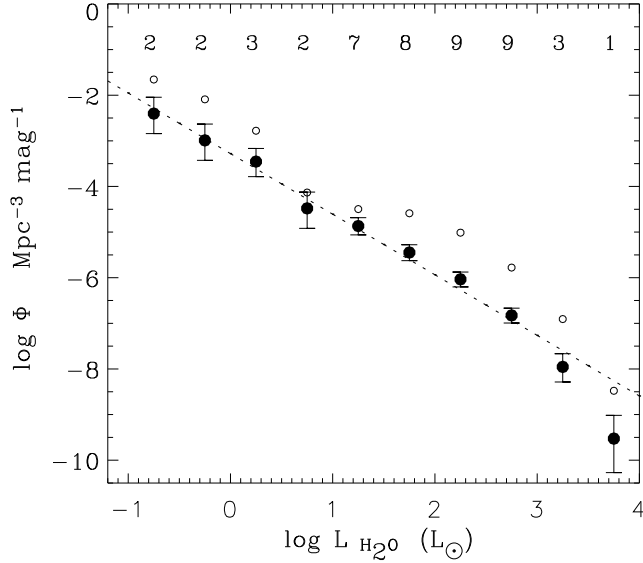


Fig. 10. The 22 GHz H₂O luminosity function (LF) for maser galaxies beyond the Magellanic Clouds (Table 4). The filled circles show the LF for a detection limit of 0.2 Jy km s^{-1} . The dashed line shows a fit with a slope of -1.3 (for uncertainties in the slope, see Sect. 4.3.2). Error bars of individual points are derived from Poisson statistics following Condon (1989). Not included in the diagram are IC 342 (too low maser luminosity) and UGC 3255, Mrk 3, Mrk 78, NGC 4151, NGC 5256 and NGC 6240 (below the adopted detection limit). The number of masing galaxies in each bin are also shown. To illustrate the effect of changing the sensitivity, we also show the LF for a detection limit of 1 Jy km s^{-1} (empty circles; in this case 19 of the 53 galaxies fall below the detection limit).

Can we hope to see H₂O megamaser emission at cosmological distances? The most luminous megamaser known at present, that in TXS2226–184 with a redshift of $z=0.025$ (Koekemoer et al. 1995), a peak flux density of 400 mJy , and a linewidth of $\sim 80 \text{ km s}^{-1}$ would be detectable by a 100-m telescope out to $z \sim 0.4$. With the Square Kilometer Array (SKA) detections at significant redshifts will thus be possible.

We may also estimate the number of detectable H₂O megamasers with the LF shown in Fig. 10. The lower limit to the H₂O luminosity of a source at distance D varies as

$$L_{\text{H}_2\text{O}} = C_1 D_{\text{max}}^2.$$

The total number of H₂O masers of a given luminosity to be detected within this distance can then be expressed by

$$N_{\text{tot,H}_2\text{O}} = \int N_{\text{H}_2\text{O}} dV_{\text{obs}} = (4/3)\pi N_{\text{H}_2\text{O}} D_{\text{max}}^3,$$

where $N_{\text{H}_2\text{O}}$ is the uniform space density of the masers. Assuming that the overall slope of the LF is independent of the maser luminosity, we then obtain with

$$N_{\text{H}_2\text{O}} = C_2 L_{\text{H}_2\text{O}}^{-1.6}$$

(see above)

$$N_{\text{tot,H}_2\text{O}} = (4/3)\pi C_1^{-1.5} C_2 L_{\text{H}_2\text{O}}^{-0.1} \propto L_{\text{H}_2\text{O}}^{-0.1}$$

This implies that the number of observable masers is almost independent of their intrinsic luminosity: The smaller source density at higher H₂O luminosities is compensated by the larger volume in which they can be detected. In principle, this would permit H₂O detections with 100-m sized telescopes out to large redshifts, provided that the LF is not steepening at very high maser luminosities and that it is possible to find suitable candidate sources.

In Sect. 4.3.1 evidence was found that only a small fraction of the detectable luminous H₂O maser sources is known to date. This may be the main cause for the comparatively steep slope in the LF at highest maser luminosities (see Fig. 10). Ignoring therefore the two bins with highest maser luminosities in Fig. 10, the slope of the LF becomes -1.3 instead of -1.6 . This provides a realistic estimate of systematic errors but does not qualitatively change our conclusion.

At the end of Sect. 4.3.1 it was mentioned that the LF is also needed to quantify the deficit of distant high luminosity masers. Adopting the result (see above) that the number of detectable masers is almost independent of the maser luminosity, we can determine with

$$V/V_{i+1} = [L_{\text{H}_2\text{O},i+1} - L_{\text{H}_2\text{O},i}]^{-1} L_{\text{H}_2\text{O},i+1}^{-1.5} \int L_{\text{H}_2\text{O}}^{1.5} dL_{\text{H}_2\text{O}}$$

the fractional volume $V_f = V/V_{i+1}$ that masers can occupy in the luminosity range $L_{\text{H}_2\text{O},i}$ to $L_{\text{H}_2\text{O},i+1}$ relative to the maximum volume V_{i+1} defined by the upper luminosity limit $L_{\text{H}_2\text{O},i+1}$. The indices i and $i+1$ indicate the lower and upper boundaries of the studied luminosity bin. The integral is calculated between the limits $L_{\text{H}_2\text{O},i}$ and $L_{\text{H}_2\text{O},i+1}$. For order of magnitude bins as considered in Sect. 4.3.1 an occupied average volume of 44% is reached. For the luminous megamasers with $L_{\text{H}_2\text{O}} \geq 100 L_\odot$ we thus expect 7% of the detections in the inner shells and 93% in the outer envelope that is still far from the observed (73% versus 27%) maser distribution. We thus conclude that the distance bias outlined in Sect. 4.3.1 is real and that the LF slope remains approximately constant within the $L_{\text{H}_2\text{O}}$ range shown in Fig. 10.

5. Conclusions

This article presents a search for 22 GHz ($\lambda \sim 1.3$ cm) H₂O masers towards two classes of objects, i.e. galaxies that (1) either contain nuclear jets that are oriented close to the disk of the galaxy and the plane of the sky or that (2) are bright in the far infrared. The main results are:

(1) Two new ‘jet-maser’ sources were detected. One of these, Mrk 1066, shows two components that bracket the systemic velocity of its parent galaxy. Mrk 34 contains the most distant and one of the most luminous megamasers so far observed in a Seyfert galaxy. The source comprises three spectral components that cover a velocity range of $\sim 1000 \text{ km s}^{-1}$.

(2) Two new masers were also detected in the sample of FIR bright galaxies. One source is a relatively weak ($L_{\text{H}_2\text{O}} \sim 1 L_\odot$) kilomaser, while the other, Arp 299, is a luminous megamaser in a merging system with high infrared luminosity. There may be two maser components, one associated with the subsystem IC 694 and the other with NGC 3690, following the conventional nomenclature of the source.

(3) When compared with other H₂O surveys, the jet-maser and FIR maser samples show extremely high detection rates and are thus providing a strong motivation for further studies. Including previously detected sources, the jet-maser detection rate is 50% (7/14), while the FIR maser detection rate is 22% (10/45).

(4) As far as one can judge from single-dish data (this paper and Braatz et al. 2004), a significant fraction of the ‘jet-maser’ sources appear to be disk-masers with a closer resemblance to NGC 4258 than to classical jet-maser sources like Mrk 348 or NGC 1052.

(5) The detection rate in the sample of bright FIR sources is a function of the FIR flux density. This implies that more sensitive surveys will detect H₂O in galaxies with smaller $100 \mu\text{m}$ fluxes. An increase in observational sensitivity by a factor of ~ 10 should yield a 25-fold increase in the number of detections.

(6) The correlation between IRAS Point Source and total H₂O luminosity of a galaxy follows, with significant scatter, the correlation found for individual star forming regions in the Galaxy. While the agreement is expected for galaxies hosting masers associated with star formation, the agreement for galaxies with AGN dominated masers is less obvious. It may be related to spatially extended dust rich cascades of bars that fuel the central engine.

(7) $60 \mu\text{m}/100 \mu\text{m}$ color temperatures from the IRAS Point Source Catalog are not correlated with H₂O maser luminosities (see footnote a) in Table 4).

(8) There is an observational distance bias: Most of the detectable luminous H₂O megamasers ($L_{\text{H}_2\text{O}} > 100 L_\odot$) have not yet been found.

(9) The extragalactic H₂O maser luminosity function (LF) might show a minimum near the transition between the luminosity range of kilomasers (mostly star formation) and megamasers (AGN) in the interval $1\text{--}10 L_\odot$. The overall slope is ~ -1.6 and implies that the number of observ-

able masers is almost independent of their luminosity. If the LF is not steepening at very high luminosities and if there is a chance to find suitable candidate sources, masers should be detectable with existing telescopes out to cosmological distances.

Acknowledgements. We wish to thank M. Elitzur and L.J. Greenhill for useful discussions during the conception of this project and an anonymous referee for carefully reading the draft and making useful suggestions. AP and AT wish to thank the MPIfR for their hospitality during the observing run. NN was partially supported by the Italian Ministry for University and Research (MURST) under grant Cofin00-02-36 and the Italian Space Agency (ASI) under grant 1/R/27/00. This research has made use of the NASA/IPAC Extragalactic Database (NED) which is operated by the Jet Propulsion Laboratory, Caltech, under contract with NASA. This research has also made use of NASA’s Astrophysics Data System Abstract Service.

References

- Aalto, S., Radford, S. J. E., Scoville, N. Z., & Sargent, A. L., 1997, *ApJ*, 475, L107
- Argon, A. L., Greenhill, L. J., Moran, J. M., et al. 1994, *ApJ*, 422, 586
- Baan, W. A., & Haschick, A. D. 1990, *ApJ*, 364, 65
- Ballo, L., Braitto, V., Della Ceca, R., et al. 2004, *ApJ*, 600, 634
- Baudry, A., Brouillet, N., & Henkel, C. 1994, *A&A*, 287, 20
- Baudry, A., & Brouillet, N. 1996, *A&A*, 316, 188
- Becker, R., Henkel, C., Wilson, T.L., & Wouterloot, J.G.A. 1993, *A&A*, 268, 483
- Bower, G., Wilson, A. S., Morse, J. A., et al. 1995, *ApJ*, 454, 106
- Braatz, J. A., Wilson, A. S., & Henkel, C. 1994, *ApJ*, 437, L99
- Braatz, J. A., Wilson, A. S., & Henkel, C. 1996, *ApJS*, 106, 51
- Braatz, J. A., Wilson, A. S., & Henkel, C. 1997, *ApJS*, 110, 321
- Braatz, J. A., Wilson, A. S., Henkel, C., Gough, R., & Sinclair, M. 2003, *ApJS*, 146, 249
- Braatz, J. A., Henkel, C., Greenhill, L. J., Moran, J. M., & Wilson, A. S. 2004, *ApJ*, 617, L29
- Brunthaler, A., Reid, M., Falcke, H., Greenhill, L. J., & Henkel, C. 2002, *Proc. 6th European VLBI Network Symposium*, eds. E. Ros et al., MPIfR, Bonn, Germany, p189
- Casoli, F., Dupraz, C., & Combes, F. 1992, *A&A*, 264, 55
- Casoli, F., Willaime, M.-C., Viallefond, F., & Gerin, M. 1999, *A&A*, 346, 663
- Churchwell, E., Witzel, A., Huchtmeier, W., et al. 1977, *A&A*, 54, 969
- Claussen, M., Heiligman, G. M., & Lo, K. Y. 1984, *Nature*, 310, 298
- Claussen, M. J., Diamond, P. J., Braatz, J. A., Wilson, A. S., & Henkel, C. 1998, *ApJL*, 500, 129
- Condon, J. J. 1989, *ApJ*, 338, 13
- Darling, J., & Giovanelli, R. 2002a, *AJ*, 124, 100
- Darling, J., & Giovanelli, R. 2002b, *ApJ*, 572, 810
- de Bruyn, A. G., & Hummel, E. 1979, *A&A*, 73, 196
- de Grijp, M. H. K., Keel, W. C., Miley, G. K., Goudfrooij, P., & Lub, J. 1992, *A&AS*, 96, 389
- Della Ceca, R., Ballo, L., Tavecchio, F., et al. 2002, *ApJ*, 581, L9
- Dos Santos, P. M. & Lépine, J. R. D. 1979, *Nature*, 278, 34

- Falcke, H., Wilson, A. S., & Simpson, C. 1998, *ApJ*, 502, 199
- Falcke, H., Henkel, C., Peck, A. B., et al. 2000, *A&A*, 358, L17
- Fiebig, D. & Güsten, R. 1989, *A&A*, 214, 333
- Fullmer, L., & Lonsdale, C. 1989, *Cataloged Galaxies and Quasars Observed in the IRAS Survey, Version 2*, JPL D-1932
- Gallais, P., Charmandaris, V. V., Le Floch, E., et al. 2004, *A&A*, 414, 845
- Gallimore, J. F., Baum, S. A., O'Dea, C. P., Brinks, E., & Pedlar, A. 1996, *ApJ*, 462, 740
- Gallimore, J. F., Henkel, C., Baum, S. A., et al. 2001, *ApJ*, 556, 694
- Gao, Y., & Solomon, P. M. 2004, *ApJS*, 152, 63
- Gardner, F. F., & Whiteoak, J. B. 1982, *MNRAS*, 201, 13p
- Gehrz, R. D., Sramek, R. A., & Weedman, D. W. 1983, *ApJ*, 267, 551
- Gimeno, G. N., Diaz, R. J., & Carranza, G. J. 2004, *AJ*, 128, 62
- Greenhill, L. J. 2002, *IAU Symp. 206, in Cosmic Masers: From Protostars to Blackholes*, eds. V. Migenes & M.J. Reid, *Astron. Soc. of the Pacific, San Francisco*, p381
- Greenhill, L. J. 2004, *New Astron. Rev.*, 48, 1079
- Greenhill, L. J., Moran, J. M., Reid, M. J., Menten, K. M., & Hirabayashi, H. 1993, *ApJ*, 406, 482
- Greenhill, L. J., Jiang, D. R., Moran, J. M., et al. 1995, *ApJ*, 440, 619
- Greenhill, L. J., Herrnstein, J. R., Moran, J. M., Menten, K. M., & Velusamy, T. 1997a, *ApJ*, 486, L15
- Greenhill, L. J., Moran, J. M., & Herrnstein, J. R. 1997b, *ApJ*, 481, L23
- Greenhill, L. J., Moran, J. M., Booth, R. S., et al. 2001, in *Galaxies and Their Constituents at the Highest Angular Resolutions*, *IAU Symposium 205*, eds. R. T. Schilizzi et al., *Astron. Soc. of the Pacific, Cambridge*, p334
- Greenhill, L. J., Ellingsen, S. P., Norris, R. P., et al. 2002, *ApJ*, 565, 836
- Greenhill, L. J., Booth, R. S., Ellingsen, S. P., et al. 2003a, *ApJ*, 590, 162
- Greenhill, L. J., Kondratko, P. T., Lovell, J. E. J., et al. 2003b, *ApJ*, 582, L11
- Hagiwara, Y., Kohno, K., Kawabe, R., & Nakai, N. 1997, *PASJ*, 49, 171
- Hagiwara, Y., Diamond, P. J., Nakai, N., & Kawabe, R. 2001a, *ApJ*, 560, 119
- Hagiwara, Y., Henkel, C., Menten, K. M., & Nakai, N. 2001b, *ApJ*, 560, L37
- Hagiwara, Y., Diamond, P. J., & Miyoshi, M., 2002, *A&A*, 383, 65
- Hagiwara, Y., Diamond, P. J., & Miyoshi, M., 2003a, *A&A*, 400, 457
- Hagiwara, Y., Diamond, P. J., Miyoshi, M., Rovilos, E., & Baan, W. A. 2003b, *MNRAS*, 344, L53
- Haschick, A. D., & Baan, W. A. 1985, *Nature*, 314, 144
- Henkel, C., & Braatz, J. A. 2003, *Acta Astron. Sinica Suppl.*, 44, 55
- Henkel, C., & Wiklind, T. 1997, *Sp. Sci. Rev.*, 81, 1
- Henkel, C., Güsten, R., Downes, D., et al. 1984, *A&A*, 141, L1
- Henkel, C., Wouterloot, J. G. A., & Bally, J. 1986, *A&A*, 155, 193 (HWB)
- Henkel, C., Wang, Y. P., Falcke, H., Wilson, A. S., & Braatz, J. A. 1998, *A&A*, 335, 463
- Henkel, C., Braatz, J. A., Greenhill, L. J., & Wilson, A. S. 2002, *A&A*, 394, L23
- Henkel, C., Tarchi, A., Menten, K. M., Peck, A. B. 2004, *A&A*, 414, 117
- Henkel, C., Braatz, J. A., Tarchi, A., et al. 2005, *ApSS*, in press (astro-ph/0407161)
- Herrnstein, J. R., Moran, J. M., Greenhill, L. J., et al. 1999, *Nature*, 400, 539
- Hibbard, J. E., & Yun, M. S. 1999, *AJ*, 118, 162
- Ho, P. T. P., Martin, R. N., Henkel, C., & Turner, J. L. 1987, *ApJ*, 320, 663
- Huchtmeier, W. K., Witzel, A., Kühr, H., Pauliny-Toth, I. I., & Roland, J. 1978, *A&A*, 64, L21
- Ishihara, Y., Nakai, N., Iyomoto, N., et al. 2001, *PASJ*, 53, 215
- Irwin, J. A., Saikia, D. J., & English, J. 2000, *AJ*, 119, 1592
- Jaffe, D. T., Güsten, R., & Downes, D. 1981, *ApJ*, 250, 621
- King, D., & Irwin, J. A. 1997, *NewA*, 2, 251
- Koekemoer, A. M., Henkel, C., Greenhill, L. J., et al. 1995, *Nature*, 378, 697
- Kylafis, N. D. & Norman, C. 1987, *ApJ*, 323, 346
- Kylafis, N. D. & Norman, C. 1991, *ApJ*, 373, 525
- Maloney, P. R. 2002, *PASA*, 19, 401
- Mauersberger, R., Wilson, T. L., & Henkel, C. 1988, *A&A*, 201, 123
- Meurs, E. J. A. & Wilson, A. S. 1984, *A&A*, 136, 206
- Miyoshi, M., Moran, J. M., Herrnstein, J. R., et al. 1995, *Nature*, 373, 127
- Morganti, R., Greenhill, L. J., Peck, A. B., Jones, D. L., Henkel, C. 2004, *New Astron. Rev.*, 48, 1195
- Nagar, N. M., & Wilson, A. S. 1999, *ApJ*, 516, 97
- Nagar, N. M., Wilson, A. S., Mulchaey, J. S., & Gallimore, J. F. 1999, *ApJS*, 120, 209
- Nakai, N., Sato, N., & Yamauchi, A. 2002, *PASJ*, 54, L27
- Peck, A. B., Henkel, C., Ulvestad, J. S., et al. 2003, *ApJ*, 590, 149
- Randell, J., Field, D., Jones, K. N., et al. 1995, *A&A*, 300, 659
- Sargent, A., & Scoville, N. Z. 1991, *ApJ*, 366, L1
- Schmidt, M. 1968, *ApJ*, 151, 393
- Shlosman, I., & Heller, C. H. 2002, *ApJ*, 565, 921
- Tarchi, A., Henkel, C., Peck, A. B., & Menten, K. M. 2002a, *A&A*, 385, 1049
- Tarchi, A., Henkel, C., Peck, A. B., & Menten, K. M. 2002b, *A&A*, 389, L39
- Tarchi, A., Henkel, C., Chiaberge, M., & Menten, K. M. 2003, *A&A*, 407, L33
- Trotter, A. S., Greenhill, L. J., Moran, J. M., et al. 1998, *ApJ*, 495, 740
- Turner, B. E. 1985, *ApJ*, 299, 312
- Ulvestad, J. S., & Wilson, A. S. 1984, *ApJ*, 278, 544
- Unger, S. W., Chapman, J. M., Cohen, R. J., Hawarden, T. G., & Mountain, C. M. 1986, *MNRAS*, 220, 1p
- Wang, Q. D., Chaves, T., & Irwin, J. A. 2003, *ApJ*, 598, 969
- Weliachew, L., Fomalont, E. B., & Greisen, E. W., 1984, *A&A*, 137, 335
- Whittle, M. 1992, *ApJS*, 79, 49
- Wilson, A. S., Braatz, J. A., & Henkel, C. 1995, *ApJ*, 455, L127
- Wouterloot, J. G. A., & Walmsley, C. M. 1986, *A&A*, 168, 237